Pergamon

Tetrahedron 55 (1999) 11365–11384

TETRAHEDRON

Recognition-Induced Control of a Diels-Alder Cycloaddition

Andrew Robertson, Douglas Philp* and Neil Spencer

School of Chemistry, University of Birmingham, Edgbaston, Birmingham B15 2TT, United Kingdom

Received 22 April 1999; revised 25 June 1999; accepted 15 July 1999

Abstract: The rational design of systems which are capable of accelerating and/or controlling the stereochemical outcome of the Diels-Alder cycloaddition reaction between a furan and a maleimide is presented. The origins of the acceleration and control of the cycloaddition reactions are traced by kinetic studies – allied to molecular mechanics calculations – to the formation of complexes in which the dienes and the dieneophiles are placed in the appropriate arrangements for reaction, and, more importantly, to the formation of intramolecular hydrogen bonds in the cycloadducts.

Keywords: Furans, Cycloaddition, Kinetics, Molecular recognition

The acceleration of chemical reactions, and the control of their regio- and/or stereochemical outcome, through the intervention of recognition processes in solution, a key component of enzymatic systems, has prompted synthetic chemists to design a variety[1] of unnatural systems which are capable of performing similar tasks.

In principle, the location of complementary recognition sites on the reactive partners in a chemical reaction permits these partners to associate with each other through their mutually compatible recognition sites. The formation of this reactive complex renders the chemical reaction between the reagents effectively intramolecular as opposed to intermolecular. Thus, one effect of the formation of the reactive complex is to shift some of the entropic cost of organising the reagents to a binding event early in the reaction sequence and, hence, we might expect such reactive complexes to effect significant rate acceleration[2,3] of chemical reactions. In addition, the use of specific recognition to preassociate the reactive partners should permit the control of the stereo- and/or regiochemical outcome of the reaction through the orientation of the reagents. These effects will manifest themselves when the reaction in question is under kinetic control and the selective stabilisation of one transition state with respect to another serves to accelerate[4] the formation of one product.

In addition, the molecular recognition which is present in the reactive complex may also persist in the final product. Thus, the noncovalent interactions which serve to preassociate the reagents may also have a profound influence on the stability of the products of the reaction. This effect will manifest itself when the reaction in

0040-4020/99/$ - see front matter
PII: S0040-4020(99)00633-X

question is under thermodynamic control and the selective stabilisation of one product with respect to another serves to facilitate[4] the formation of the more stable product.

We have become interested[5] in the possibility of achieving acceleration and control in solution phase reaction processes through the use of molecular recognition. In particular, we wished to investigate the acceleration[6] and control[7] of the Diels-Alder reaction between a maleimide and a furan. In principle, this reaction can give rise to two products – the *endo* adduct and the *exo* adduct – depending on the orientation of the approach of the diene to the dienophile. Normally, the *endo* adduct is the kinetic product and the *exo* adduct is the thermodynamic product of this reaction. One method of achieving rate acceleration[8] involves transforming the bimolecular reaction between the diene and dienophile in solution into a unimolecular reaction within a non-covalently bound complex.

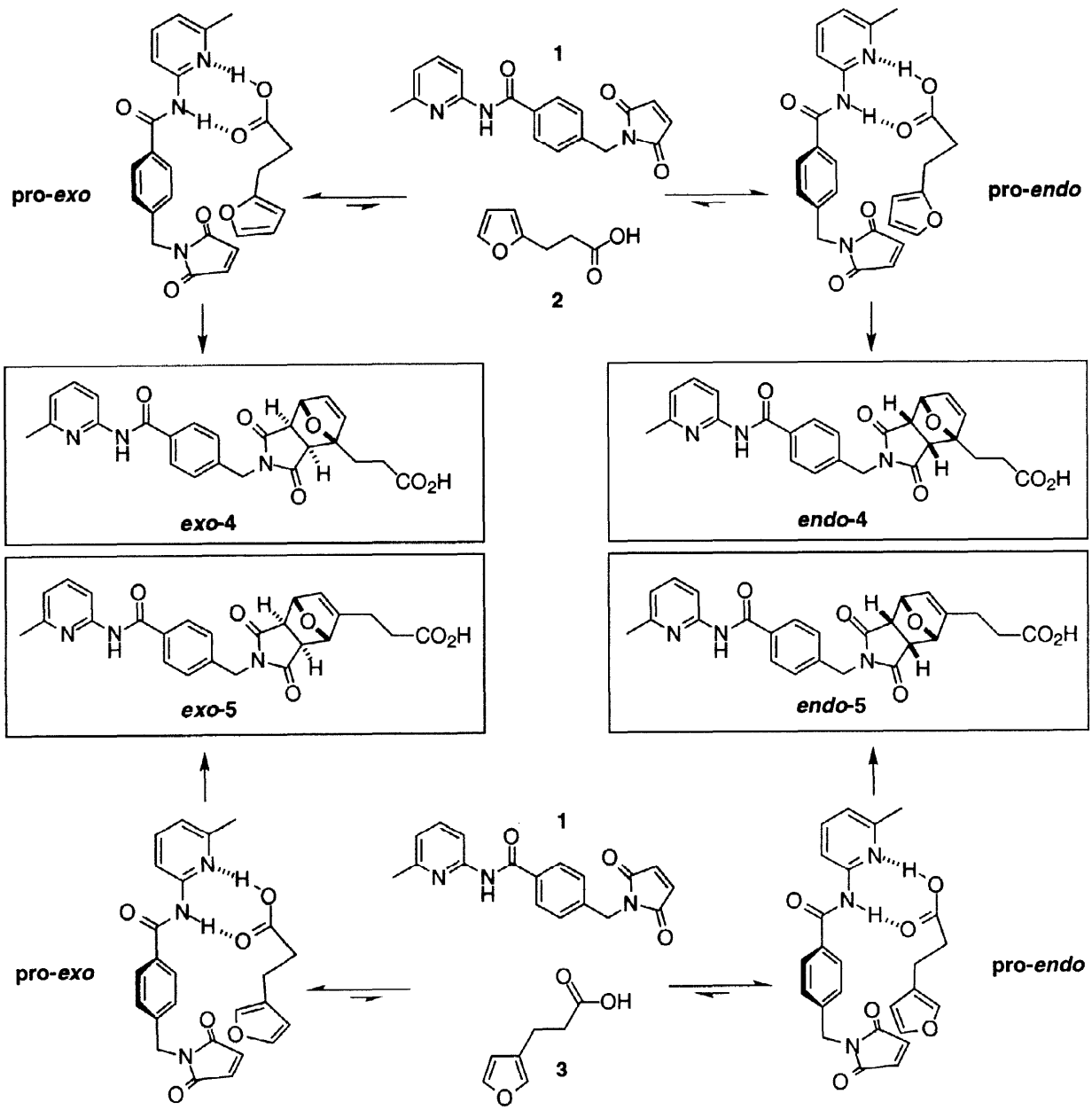

Figure 1 – Design of a recognition-based system for the control and acceleration of a Diels-Alder cycloaddition.

This can be accomplished most readily by locating complementary recognition sites on the diene and dienophile. Accordingly, we designed (Figure 1) the maleimide **1**, which bears an amidopicoline moiety, and the furans **2** and **3**, which both bear a carboxylic acid. The mutual recognition between the amidopicoline and the carboxylic acids should permit the formation of the [**1**•**2**] and [**1**•**3**] complexes (Figure 1) which could adopt structures in which the furan and maleimide rings are disposed in either a pro-*endo* or a pro-*exo* orientation (Figure 1). Thus, we might expect the rate of the cycloaddition would be accelerated by the formation of these complexes through the mechanisms discussed above. Additionally, we wished to probe how the stereochemistry of the cycloadduct would be affected by the interplay between the stabilities of the pro-*endo* and pro-*exo* orientations in the [**1**•**2**] and [**1**•**3**] complexes and the presence, or absence, of hydrogen bonding in the respective products, ***endo***- and ***exo***-**4** and ***endo***- and ***exo***-**5**. The use of the isomeric furans **2** and **3** allows us to probe how differences in the accessible conformational space of the products affect their ability to form intramolecular hydrogen bonds and, hence, affect the relative stabilities of the *endo* and *exo* isomers of **4** and **5**.

Here, we report the following: (i) syntheses of **1**, **2** and **3** (ii) the observation of an accelerated Diels-Alder reaction between **1** and **2** and an accelerated and controlled Diels-Alder reaction between **1** and **3** and (iii) the rationalisation and analysis of this behaviour by kinetic simulation and molecular mechanics calculations.

The preparation of the target maleimide **1** was accomplished in five steps (Scheme 1) starting from commercially-available 4-(aminomethyl)benzoic acid. The amino group of 4-(aminomethyl)benzoic acid was protected as the corresponding benzyl carbamate **6** by treatment[9] with benzyl chloroformate in aqueous K_2CO_3 solution. For convenience, the potassium salt of **6** was isolated and used in the subsequent transformation. Treatment of **6** with neat $SOCl_2$ at room temperature afforded **7** in good yield and the acid chloride could then be condensed with 2-amino-6-methylpyridine to afford the amidopyridine **8**.

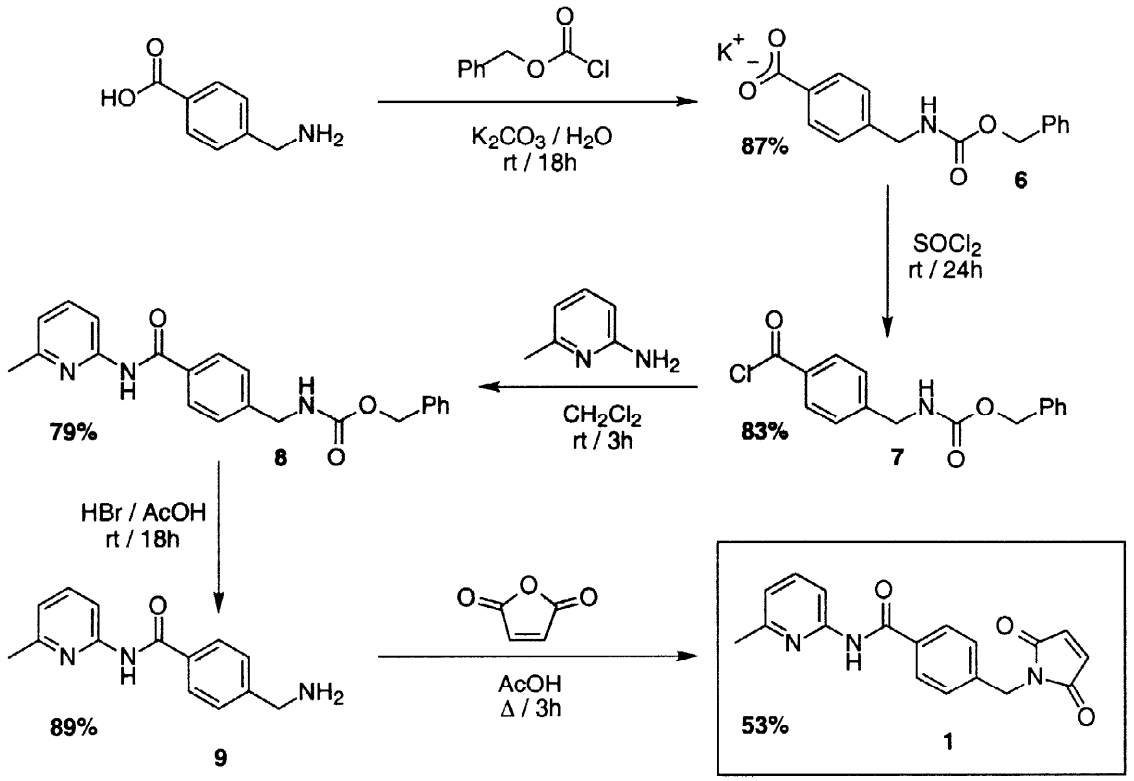

Scheme 1

Deprotection of **8** was achieved by treatment with HBr in AcOH followed by neutralisation with aqueous NaOH solution affording the free amine **9**. The target maleimide **1** was prepared by reacting amine **9** with maleic anhydride in glacial acetic acid.

The target dienes **2** and **3** were prepared (Scheme 2) by hydrogenation of the corresponding commercially-available furylacrylic acids.

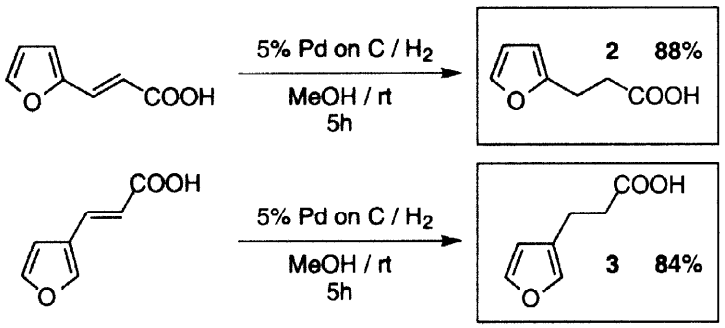

Scheme 2

In order to make effective comparisons between the recognition-mediated reaction and the intermolecular reaction channel, it was necessary to identify a control compound, which did not possess any recognition sites, to assess the bimolecular reactivity of the maleimide **1**. Accordingly, we selected benzyl maleimide **10** as this control compound and this material was synthesised readily (Scheme 3) starting from benzylamine.

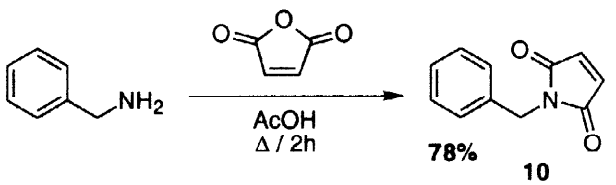

Scheme 3

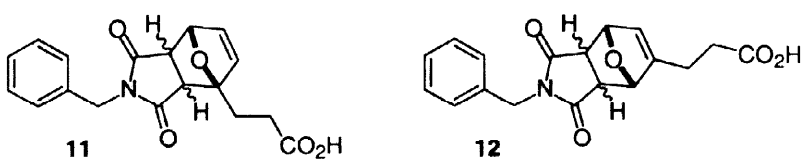

In order to assess the efficiency of the rate acceleration and control induced by the formation of a complex between **1** and **2**, we followed the course of the reaction between these components in $CDCl_3$ at 30°C. The initial concentrations of the reactants were 5 mM and the emergence of the resonances in the region δ 5.10 to δ 5.30, arising from the bridgehead protons[10] in ***exo*-4** and ***endo*-4**, were monitored by 400 MHz ^{1}H NMR spectroscopy over a period of 60 hours. The reaction between **2** and benzyl maleimide was chosen as the control reaction and was performed and monitored under identical conditions observing the appearance of ***endo*-** and ***exo*-11**. The data obtained (Figure 2) indicates that the recognition-mediated (RM) reaction proceeds slightly faster than the control reaction at this concentration. The kinetic data for the control reaction were used to extract estimates for the bimolecular rate constants k_1 through k_4. These estimates for k_1 through k_4, together with the

association constant for the [1•2] complex, determined by ^{1}H NMR dilution experiments, were then used to perform simulations of the kinetic behaviour of the recognition-mediated system by numerical integration of the rate equations derived from the model shown in Figure 3. Best fit values of the rate constants for the recognition-mediated reaction (Table 1) were then calculated using non-linear least-squares fitting of the model parameters k_5 through k_8 (Figure 3) using simplex and Newton-Raphson methods coupled with simulations of the rate profile of the recognition-mediated system. These simulations using the values of the rate constants in Table 1 give acceptable agreement between the calculated rate profile and the experimental data (Figure 2).

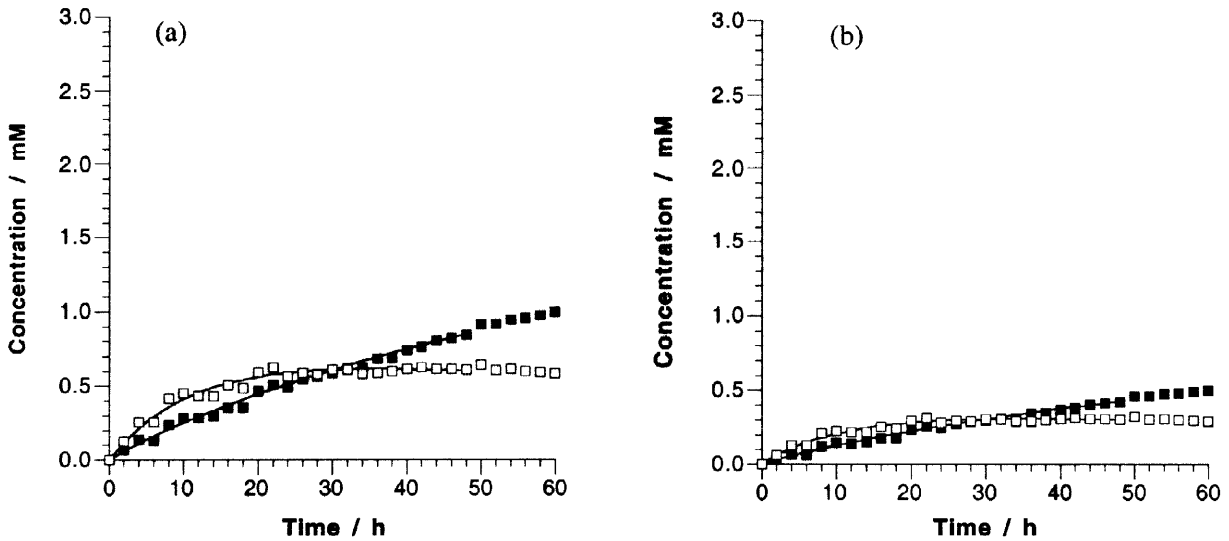

Figure 2 – Rate profiles for (a) the reaction between **1** and **2** in $CDCl_3$ at 30°C and (b) the reaction between benzyl maleimide and **2** in $CDCl_3$ at 30°C. In both cases, the starting concentrations of the reactants were 5 mM. In both plots, the filled squares represent the concentration of the appropriate *exo* cycloadduct and the open squares represent the concentration of the appropriate *endo* cycloadduct. The solid lines represent the best fit of the appropriate kinetic model to the experimental data. For clarity, error bars are omitted from the graphs, however, errors in concentration are estimated to be ±7%.

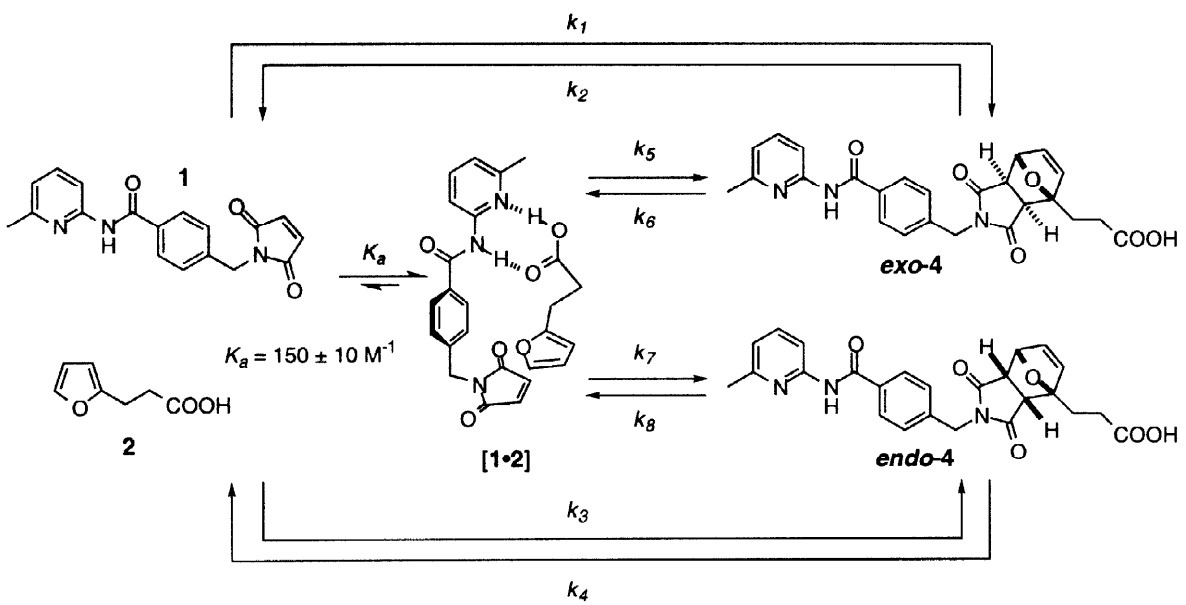

Figure 3 – Kinetic model for the reaction between **1** and **2**.

Table 1 – Kinetic parameters for the recognition-mediated reaction between **1** and **2** obtained from the simulation and fitting of the kinetic model shown in Figure 3 to the experimental data.

k_1 / 10^{-6} $M^{-1}s^{-1}$	146 ± 7	k_5 / 10^{-6} s^{-1}	3.59 ± 0.11
k_2 / 10^{-6} s^{-1}	0.975 ± 0.03	k_6 / 10^{-6} s^{-1}	0.063 ± 0.004
k_3 / 10^{-6} $M^{-1}s^{-1}$	214 ± 8	k_7 / 10^{-6} s^{-1}	9.17 ± 0.21
k_4 / 10^{-6} s^{-1}	16.0 ± 0.17	k_8 / 10^{-6} s^{-1}	1.90 ± 0.06

It is clear from the kinetic data that both the control and recognition-mediated cycloaddition reactions are reversible under the reaction conditions employed and, therefore, the reaction will be under thermodynamic control. It also clear from the kinetic data that, although the *endo* cycloadduct is the kinetic product of the reaction, the *exo* cycloadduct is the thermodynamic product of both the control and recognition-mediated reactions. Since the reactions are under thermodynamic control, it is appropriate to examine the effect of introducing the recognition sites into the reagents on the outcome of the reaction in terms of equilibrium constants. Table 2 gives the relevant equilibrium constants for the control (K_{bi}) and recognition-mediated (K_{RM}) processes calculated from the results of the kinetic study.

Table 2 — Equilibrium constants for the formation of *endo* and *exo* adducts from the reaction between **2** and **10** (K_{bi}) and for the recognition-mediated reaction between **1** and **2** (K_{RM}) obtained from the kinetic data given in Table 1.

$K_{bi}(exo)$ / M^{-1}	149.7	$K_{RM}(exo)$	56.89
$K_{bi}(endo)$ / M^{-1}	13.38	$K_{RM}(endo)$	4.826

Interestingly, the degree of *exo* selectivity at equilibrium is almost identical for both pathways – 11.2:1 (*exo*:*endo*) for the bimolecular process and 11.8:1 for the recognition-mediated process. This result implies that the recognition processes are not having a significant effect on the stereochemical outcome of the reaction. This inference is confirmed when we examine the thermodynamic profile for the reaction (Figure 4). The energy difference between the *exo* and *endo* products is almost the same for each pathway (6.1 $kJmol^{-1}$ for the bimolecular reaction *vs.* 6.2 $kJmol^{-1}$ in the recognition-mediated case). However, in terms of overall stability, *i.e.* compared with uncomplexed reagents, both cycloadducts are significantly more stable than those derived from the purely bimolecular system. This additional stabilisation will express itself as an increased extent of reaction under the reaction conditions used and is best expressed in terms of an effective molarity[11] (EM). Thus, the thermodynamic or equilibrium EMs for ***exo*-4** and ***endo*-4** are 380 mM and 360 mM, respectively. These values are consistent with the small increase in the extent of the reaction observed at 5 mM in $CDCl_3$ at 30°C.

Whilst the presence of hydrogen bonding in the cycloadducts ***exo*-4** and ***endo*-4** affects the position of the equilibria concerned, the role of any rate acceleration mediated by the **[1•2]** complex will express itself as a change in the rate at which equilibrium is reached. Once again, it is convenient to consider the effect of the formation of the **[1•2]** complex in terms of the effective molarities achieved within the complex for the formation of the two cycloadducts. Hence, we can derive values of 25 mM for the kinetic effective molarity achieved within the **[1•2]** complex for the formation of ***exo*-4** and 43 mM for the kinetic effective molarity achieved within the **[1•2]** complex for the formation of ***endo*-4**. Both of these values are consistent with the activation energy for the cycloaddition reaction within the complex being higher[12] than that for the bimolecular process, however, since the reaction is performed at a concentration which is less than the EM, some modest acceleration[13] will be observed.

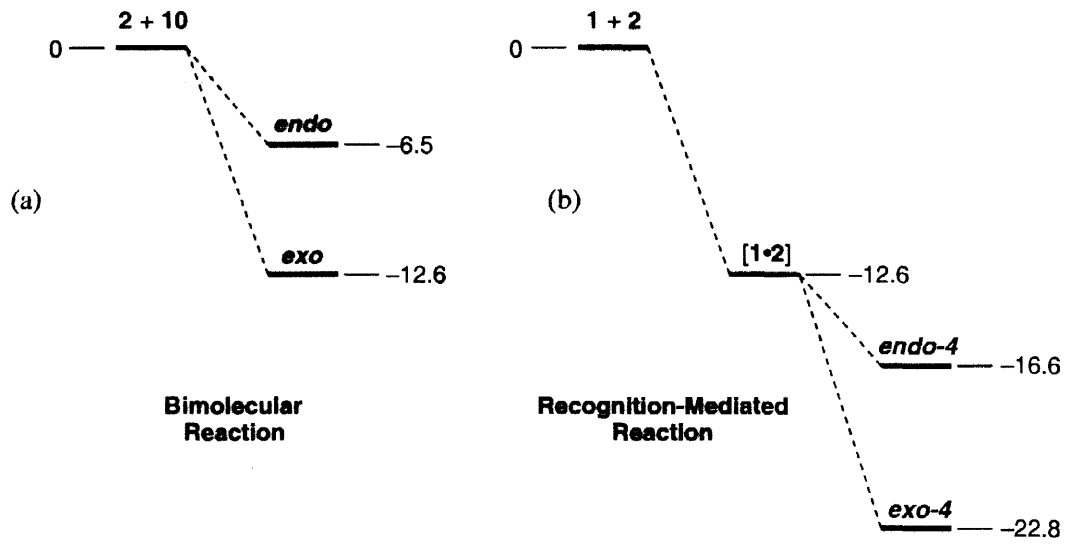

Figure 4 – Thermodynamic profile for the reaction of (a) **10** and **2** and (b) **1** and **2**. The zero point for energy comparisons is set at the energy of the uncomplexed reactants. All energy values are in kJmol^{-1}.

These results suggest that, although hydrogen bonding present in ***exo*-4** and ***endo*-4** is responsible for an increased extent of reaction between **1** and **2** at 5 mM in $CDCl_3$ at 30°C, the molecular recognition between **1** and **2** is incapable of either accelerating the reaction significantly, through the [**1•2**] complex, or controlling the stereochemical outcome of the reaction, through discrimination of the energies of the products.

In order to investigate how differences in the accessible conformational space of the *endo* and *exo* cycloadducts affects their ability to form intramolecular hydrogen bonds and, hence, affect their relative stabilities, we turned to the reaction between **1** and **3**. It was anticipated that the *endo* and *exo* cycloadducts derived from the reaction between **1** and **3** would have significantly different conformational behaviour to those derived from the reaction between **1** and **2** and, hence, rather different capacities to form intramolecular hydrogen bonds. Hence, the efficiency of the rate acceleration and control induced by the formation of a complex between **1** and **3** was assessed by following the course of the reaction between **1** and **3** in $CDCl_3$ at 30°C. The initial concentrations of the reactants were 5 mM and the emergence of the resonances in the region δ 5.10 to δ 5.30, arising from the bridgehead protons in ***exo*-5** and ***endo*-5**, were monitored by 400 MHz ^{1}H NMR spectroscopy over a period of 60 hours. Once again, the reaction between **1** and benzyl maleimide was chosen as the control reaction and this reaction was performed and monitored under identical conditions. The concentration-time data obtained from the NMR data (Figure 5) demonstrates that the recognition-mediated (RM) reaction proceeds significantly faster than the control reaction at a concentration of 5 mM and proceeds with high selectivity for ***endo*-5**. The kinetic data for the control reaction were used to extract estimates for the bimolecular rate constants k_1 through k_4. These estimates for k_1 through k_4, together with the association constant for the [**1•3**] complex, were then used to perform simulations of the kinetic behaviour of the recognition-mediated system by numerical integration of the rate equations derived from the model shown in Figure 6. Best fit values of the rate constants for the recognition-mediated reaction (Table 3) were then calculated using non-linear least-squares fitting of the model parameters k_5 through k_8 (Figure 6) using simplex and Newton-Raphson methods coupled with simulations of the kinetic behaviour of the recognition-mediated system. These simulations using the values of the rate constants in Table 3 give good agreement between the calculated rate profile and the experimental data (Figure 5).

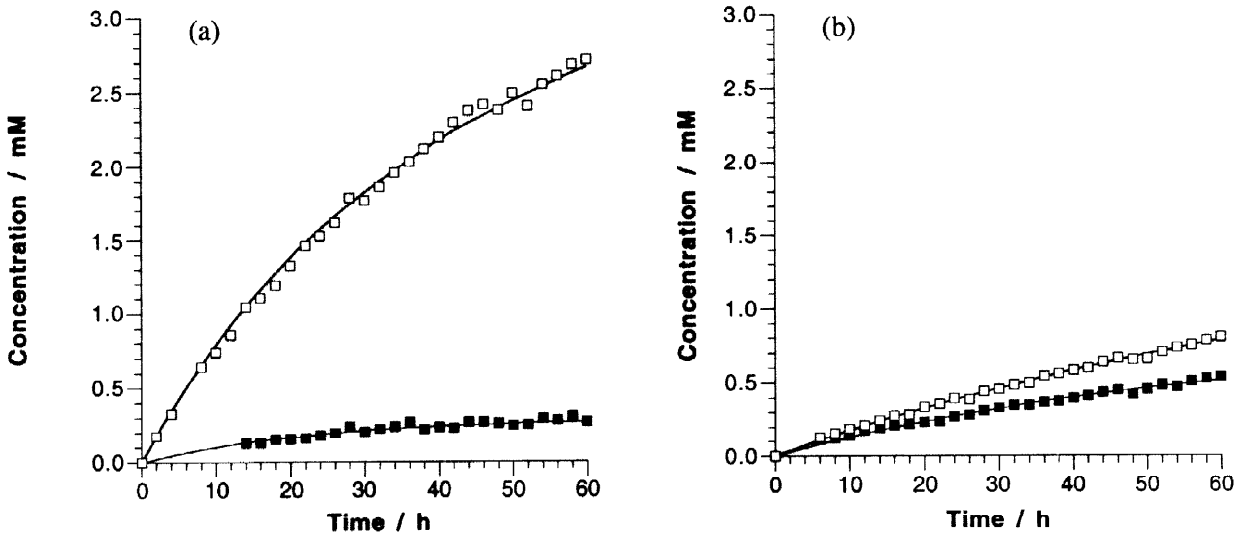

Figure 5 – Rate profiles for (a) the reaction between **1** and **3** in $CDCl_3$ at 30°C and (b) the reaction between benzyl maleimide and **3** in $CDCl_3$ at 30°C. In both cases, the starting concentrations of the reactants were 5 mM. In both plots, the filled squares represent the concentration of the appropriate *exo* cycloadduct and the open squares represent the concentration of the appropriate *endo* cycloadduct. The solid lines represent the best fit of the appropriate kinetic model to the experimental data. For clarity, error bars are omitted from the graphs, however, errors in concentration are estimated to be ±3%.

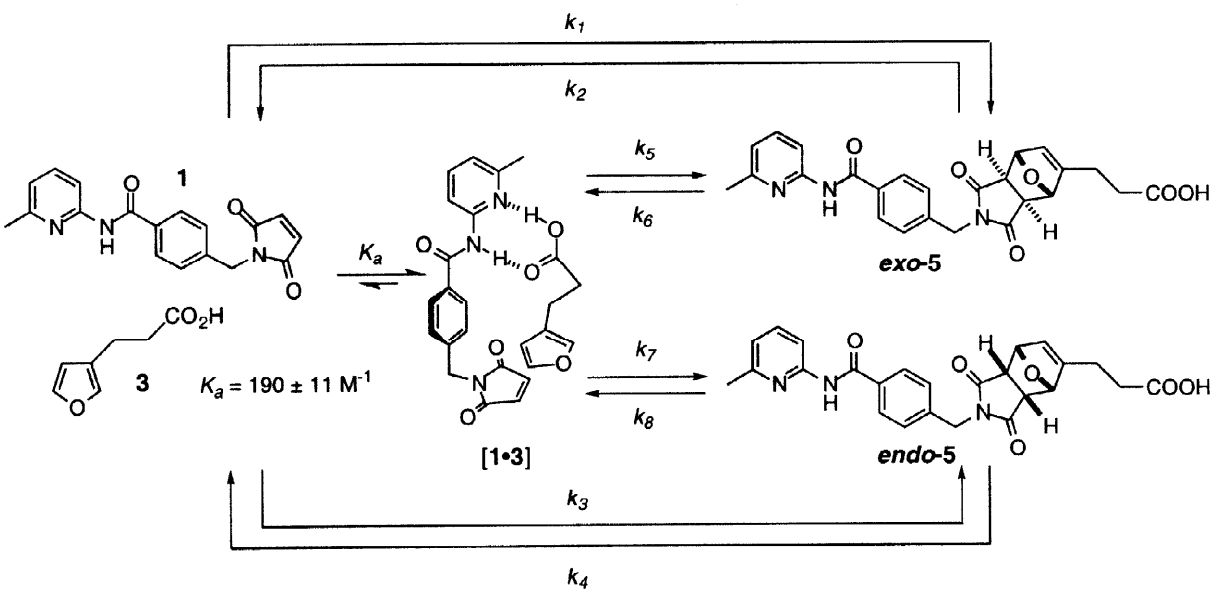

Figure 6 – Kinetic model for the reaction between **1** and **3**.

Table 3 — Kinetic parameters for the recognition-mediated reaction between **1** and **3** obtained from the simulation and fitting of the kinetic model shown in Figure 6 to the experimental data.

k_1 / 10^{-6} $M^{-1}s^{-1}$	160 ± 3	k_5 / 10^{-6} s^{-1}	0.997 ± 0.06
k_2 / 10^{-6} s^{-1}	1.67 ± 0.11	k_6 / 10^{-6} s^{-1}	0.887 ± 0.04
k_3 / 10^{-6} $M^{-1}s^{-1}$	209 ± 4	k_7 / 10^{-6} s^{-1}	13.1 ± 0.11
k_4 / 10^{-6} s^{-1}	0.329 ± 0.03	k_8 / 10^{-6} s^{-1}	0.002

Once again, it is clear from the kinetic data that both the control and recognition-mediated cycloaddition reactions are reversible under the reaction conditions used and therefore the reaction will be under thermodynamic control. Interestingly, in contrast to the cycloadditions involving furan **2**, in this case, the *endo* cycloadduct is both the kinetic and the thermodynamic product of both the control[14] and recognition-mediated reactions. As before, it is appropriate to examine the effect of introducing the recognition sites into the reagents on the outcome of the reaction in terms of equilibrium constants.

Table 4 gives the relevant equilibrium constants for the control (K_{bi}) and recognition-mediated (K_{RM}) processes calculated from the results of the kinetic studies on the control reactions between **10** and **3** and **1** and **3**.

Table 4 — Equilibrium constants for the formation of *endo* and *exo* adducts from the reaction between **3** and **10** (K_{bi}) and for the recognition-mediated reaction between **1** and **3** (K_{RM}) obtained from the kinetic data given in Table 3.

$K_{bi}(exo)$ / M^{-1}	95.8	$K_{RM}(exo)$	1.12
$K_{bi}(endo)$ / M^{-1}	635	$K_{RM}(endo)$	6650

It is clear from these data that the *endo* adduct is the thermodynamic product of both the bimolecular and the recognition-mediated pathways. However, the degree of *endo* selectivity at equilibrium is dramatically different for the two pathways – an *endo*:*exo* ratio of 6.6:1 for the control reaction becomes 5940:1 for the recognition-mediated process. This result implies that the recognition processes have a profound effect on the stereochemical outcome of the reaction. This inference is confirmed when we examine the thermodynamic profile for the reaction (Figure 7). The energy difference between the *exo* and *endo* products is 4.7 $kJmol^{-1}$ for the control reaction, with the *endo* cycloadduct being the more stable. However, in the case of the recognition-mediated reaction, the difference in stability between the *exo* and *endo* products is now 21.9 $kJmol^{-1}$.

Additionally, in terms of overall stability, *i.e.* compared with uncomplexed reagents, only the *endo* cycloadduct is significantly more stable than those derived from the purely bimolecular control reaction. This additional stabilisation will express itself as an increased extent of reaction under the reaction conditions used and is best expressed in terms of an effective molarity (EM). Thus, the thermodynamic or equilibrium EMs for ***exo*-5** and ***endo*-5** are 11.2 mM and 10310 mM, or 10.31 M, respectively. These values are consistent with the increase in the extent of the reaction observed at 5 mM in $CDCl_3$ at 30°C.

Whilst the presence of hydrogen bonding in the cycloadducts ***exo*-5** and ***endo*-5** affects significantly the positions of the equilibria concerned, as before, the role of any rate acceleration mediated by the **[1•3]** complex is to change the rate at which equilibrium is reached. Hence, we can derive values of 6 mM for the kinetic effective molarity achieved within the **[1•3]** complex for the formation of ***exo*-5** and 63 mM for the effective molarity achieved within the **[1•3]** complex for the formation of ***endo*-5**. Both of these values are consistent with the activation energy for the cycloaddition reaction within the complex being higher than that for the bimolecular process, however, since the reaction is performed at a concentration which is less than the EM for ***endo*-5**, a modest acceleration of the rate of this compound is observed.

These results suggest that the hydrogen bonding present in ***endo*-5** is responsible for an increased extent and rate of reaction between **1** and **3** at 5 mM in $CDCl_3$ at 30°C. However, it would appear that the molecular recognition between **1** and **3** is incapable of either increasing significantly the rate or the extent of the reaction leading to ***exo*-5**. This result suggests that ***exo*-5** is incapable of forming intramolecular hydrogen bonds and that

the [1•3] complex is incapable of accelerating the formation of ***exo*-5** efficiently. These two factors combine to almost completely control the relative stereochemical outcome of the cycloaddition reaction.

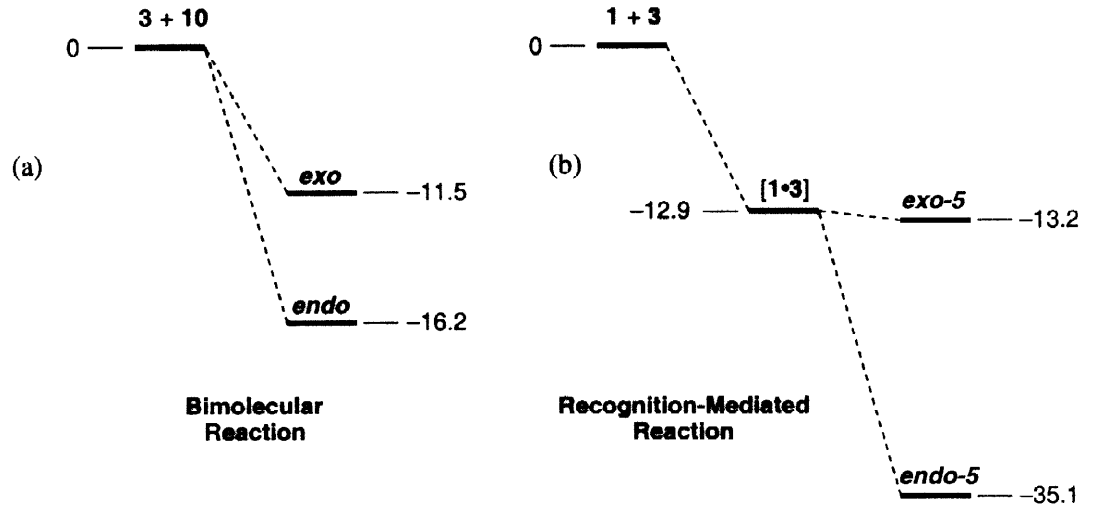

Figure 7 – Thermodynamic profile for the reaction of (a) **10** and **3** and (b) **1** and **3**. The zero point for energy comparisons is set at the energy of the uncomplexed reactants. All energy values are in kJmol^{-1}.

In order to gain further insight into the role of noncovalent interactions in influencing the outcome of the reactions between **1** and **2** and **1** and **3**, we performed a series of molecular mechanics calculations in order to elucidate the minimum energy structures of the products, ***endo*-** and ***exo*-4** and ***endo*-** and ***exo*-5**. In particular, we wished to elucidate how the abilities of the four cycloadducts to form intramolecular hydrogen bonds differed.

Accordingly, a representative set of low energy conformations for the cycloadducts ***endo*-4** and ***exo*-4** were generated using Monte Carlo conformational searching and the resultant structures were minimised using the AMBER* forcefield. Conformations which had energies more than 50 kJ from the global minimum were rejected during the search. The conformational search afforded a set of conformations which were sorted on the basis of energy.

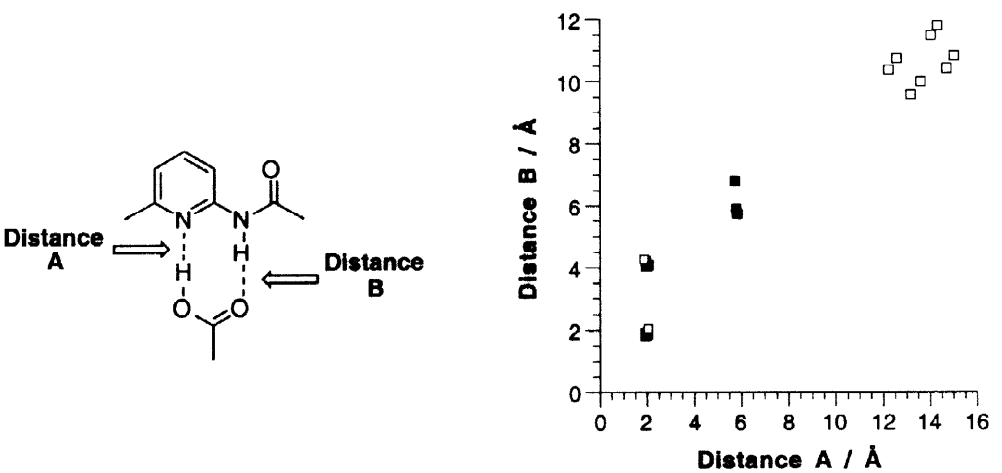

Figure 8 – Structures of the ten lowest energy conformations of ***exo*-** and ***endo*-4** expressed as functions of key hydrogen bond distances. Filled squares represent the locations of conformations of ***exo*-4** and open squares represent the locations of conformations of ***endo*-4**.

The distances (Figure 8) between the pyridine nitrogen atom and the carboxylic acid proton, and the amide proton and the carboxylic acid carbonyl oxygen atom were determined for the ten lowest energy conformations. This data was used to generate a scatterplot (Figure 8) in which the locations of individual conformations are plotted as a function of these two distances.

It is clear from the data presented in Figure 8 that the lowest energy conformations for the cycloadducts ***endo*-4** and ***exo*-4** can occupy common regions of conformational space. In particular, it is noteworthy that both cycloadducts are capable of forming intramolecular hydrogen bonds. However, for the *exo* cycloadduct, most of the minimum energy conformations contain intramolecular hydrogen bonds, whereas for the *endo* cycloadduct only two out of ten of the lowest energy conformations contain intramolecular hydrogen bonds. This observation is consistent with the thermodynamic data which suggests that ***exo*-4** is more stable than ***endo*-4**.

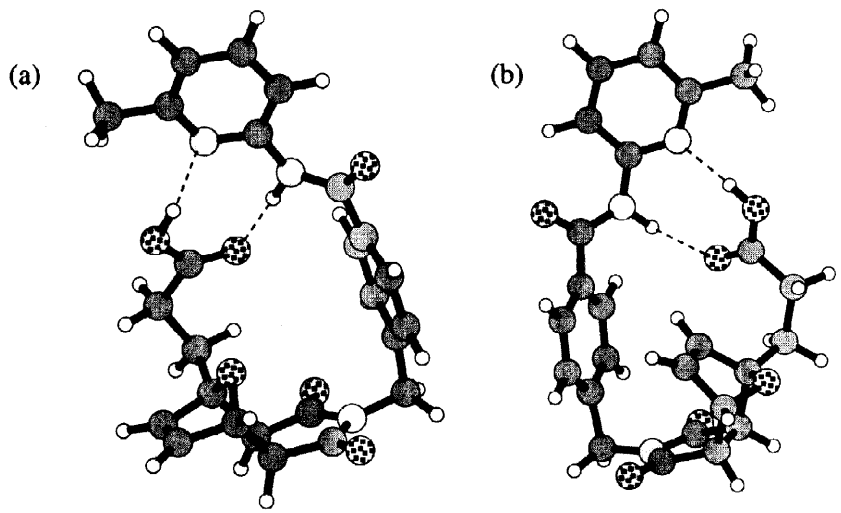

Figure 9 – Representative low energy structures for cycloadduct **4** showing (a) the *exo* isomer and (b) the *endo* isomer. In both structures, carbon atoms are shaded dark grey, nitrogen atoms are shaded light grey, oxygen atoms are speckled and hydrogen atoms are unshaded. Hydrogen bonds are marked by dashed lines.

A representative set of low energy conformations for the cycloadducts ***endo*-5** and ***exo*-5** were generated using Monte Carlo conformational searching and the resultant structures were minimised using the AMBER* forcefield. Conformations which had energies more than 50 kJ from the global minimum were rejected during the search. The conformational search afforded a set of conformations which were sorted on the basis of energy. The distances (Figure 10) between the pyridine nitrogen atom and the carboxylic acid proton, and the amide proton and the carboxylic acid carbonyl oxygen atom were determined for the ten lowest energy conformations. This data was used to generate a scatterplot (Figure 10) in which the locations of individual conformations are plotted as a function of these two distances. It is clear from Figure 10 that the low energy conformations for the cycloadducts ***endo*-5** and ***exo*-5** occupy quite different regions of conformational space. These results indicate that cycloadduct ***exo*-5** prefers to adopt extended conformations in which there are no intramolecular hydrogen bonds present in the structure – Figure 11a shows the lowest energy conformation. This observation is consistent with the results of our kinetic studies which show that the *exo* adduct does not gain any stability from the introduction of recognition sites into the diene and the dienophile. By contrast, cycloadduct ***endo*-5** prefers conformations in which there is at least one hydrogen bond present in the structure – Figure 11b shows the

lowest energy conformation in which there are two intramolecular hydrogen bonds. Interestingly, the conformations which have only one hydrogen bond only contain hydrogen bonds formed between the pyridine nitrogen atom and the carboxylic acid proton. These results are entirely consistent with and serve to reinforce the conclusion drawn from our kinetic studies which show that the *endo* adduct accrues significant stabilisation from the presence of recognition within the cycloadduct.

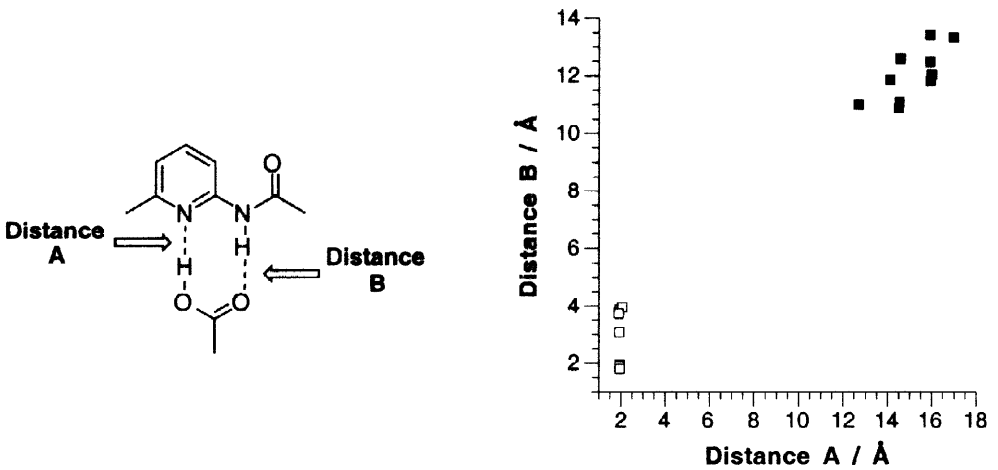

Figure 10 – Structures of the ten lowest energy conformations of ***exo***- and ***endo*-5** expressed as functions of key hydrogen bond distances. Filled squares represent the locations of conformations of ***exo*-5** and open squares represent the locations of conformations of ***endo*-5**.

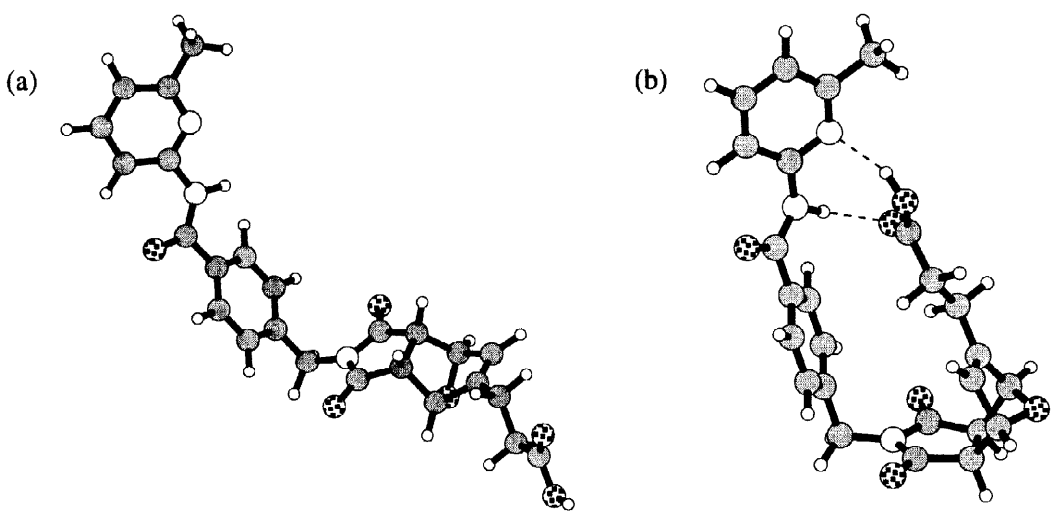

Figure 11 – Representative low energy structures for cycloadduct **5** showing (a) the *exo* isomer and (b) the *endo* isomer. In both structures, carbon atoms are shaded dark grey, nitrogen atoms are shaded light grey, oxygen atoms are speckled and hydrogen atoms are unshaded. Hydrogen bonds are marked by dashed lines.

Strong experimental evidence for the existence of the intramolecular hydrogen bonds in the cycloadducts **4** and **5**, predicted by molecular mechanics calculations, comes from ^{1}H NMR spectroscopy. For cycloadduct **4**, both *endo* and *exo* stereoisomers show strong downfield shifts of the resonances arising from the amide NH protons which are consistent with the amide proton participating in a hydrogen bond with the carbonyl oxygen of the carboxylic acid. For cycloadduct **5**, only the *endo* stereoisomer exhibits a strong downfield shift[15] of the

resonance arising from the amide NH proton (δ_{NH}(*endo*) 11.93; δ_{NH}(*exo*) 10.46). This observation is in complete accord with the molecular mechanics calculations which predict that only the *endo* stereoisomer can participate in an intramolecular hydrogen bond between the amide NH and the carbonyl oxygen of the carboxylic acid.

In summary, we have demonstrated that it is possible to facilitate and control the outcome of a Diels-Alder reaction through the attachment of appropriate recognition sites to the diene and dienophile.

The recognition-mediated reaction between **1** and **2** displays no enhancement of the stereoselectivity and minimal rate acceleration when compared to the control reaction between **10** and **2**. The lack of enhancement of the stereoselectivity can be attributed to the fact that both ***endo*-4** and ***exo*-4** are capable of exploiting intramolecular hydrogen bonds in order to stabilise themselves and, hence, the formation of both products is facilitated to approximately the same degree. The **[1•2]** complex plays little, if any, role in the outcome of the reaction since it is incapable of accelerating the formation of ***endo*-4** and ***exo*-4** significantly.

The recognition-mediated reaction between **1** and **3** displays a dramatic enhancement of the stereoselectivity and modest rate acceleration when compared to the control reaction between **10** and **3**. This enhancement of the stereoselectivity of the reaction can be attributed to the fact that only ***endo*-4** is capable of exploiting intramolecular hydrogen bonds in order to stabilise itself and, hence, the formation of this product is facilitated to a high degree (thermodynamic EM = 10.3 M). Once again, the **[1•3]** complex plays little role in the outcome of the reaction since, although it does accelerate the formation of ***endo*-5** and ***exo*-5** differentially, the effect observed is extremely modest.

We are currently addressing the problem of the efficiency of the reactive complex and exploiting the methodology set out above in the regio- and stereocontrol of other [4+2] and [3+2] cycloaddition reactions.

Experimental Section

General Procedures

All commercially-available chemicals were used as supplied except where specified. Solvents were purchased from Fisons and used as supplied except where specified. When required, solvents were distilled and dried according to literature procedures[16]: dichloromethane, toluene and benzene from calcium hydride; tetrahydrofuran, 1,4-dioxane and diethyl ether from sodium and benzophenone; dimethylformamide and methanol from magnesium sulfate and acetic acid from acetic anhydride. Nitrogen gas was dried by passage along a column of self-indicating silica gel and calcium chloride. Thin layer chromatography was performed on aluminium plates coated with either silica gel ($60F_{254}$ Merck 5554) or neutral alumina ($60F_{254}$ Merck 5550) containing fluorescent indicator. Plates were air-dried before being examined under a UV lamp (366 nm). Column chromatography was performed on silica gel (230-400 mesh, Merck 9385). Melting points were determined using an Electrothermal 9200 apparatus and are uncorrected. Electron impact mass spectrometry was carried out on a VG ProSpec mass spectrometer and fast atom bombardment and high resolution mass spectrometry were performed on a VG ZabSpec mass spectrometer. ^{1}H Nuclear magnetic resonance (NMR) spectra were recorded on Jeol GX270 (270 MHz), Bruker AC300 (300 MHz), or Bruker AMX400 (400 MHz) spectrometers using the deuterated solvent as lock and residual solvent as internal reference. ^{13}C NMR spectra were recorded on a Bruker AC300 (75 MHz) spectrometer using the deuterated solvent as lock and residual solvent as internal reference.

Kinetic Measurements

100 mM stock solutions were prepared by dissolving 1 mmol of the relevant compound in 10 ml $CDCl_3$ using 10 ml (± 0.02 ml) volumetric flasks. Stock solutions were stored at −18°C and sealed under N_2. Experimental samples were obtained by diluting the appropriate volumes of stock solutions to 1 ml total volume with $CDCl_3$ using a Hamilton 1 ml gas tight syringe or with a Hamilton 250 μl gas-tight syringe if required. Samples were mixed and monitored immediately by 400 MHz ^{1}H NMR spectroscopy. Simulation and fitting of the resultant data to the appropriate kinetic models was accomplished using the SimFit[17] program.

Association Constants

Binding constants were determined by the ^{1}H NMR dilution method[18]. Equimolar solutions of maleimide **1** and either 2-furylpropionic acid **2** or 3-furylpropionic acid **3** were prepared at concentrations from 50 mM to 2.5 mM and the resulting solutions were analysed by 270 MHz ^{1}H NMR spectroscopy. All experiments were conducted at 30°C and solutions were replaced after 30 minutes to minimise errors arising from reaction between **1** and either **2** or **3**. The change in the chemical shift of the amide proton of **1** was monitored and plotted against concentration of the solution. Data was analysed by least squares non-linear regression[19] by fitting to the equation:

$$\delta_{obs} = \delta_u + \Delta\delta\left[1 + \frac{K_d}{2c_o} - \sqrt{\left(\frac{K_d}{2c_o}\right)^2 + \frac{K_d}{c_o}}\right]$$

where δ_{obs} is the chemical shift of the observed signal at concentration C_0, δ_u is the chemical shift of the unbound species, $\Delta\delta$ the maximum change in the observed chemical shift and K_d the dissociation constant of the complex. By this method, the association constant, K_a ($1/K_d$), for the complex [**1**•**2**] was determined as 150 ± 10 M^{-1} and the association constant for the complex [**1**•**3**] was determined as 190 ± 11 M^{-1}.

Molecular Mechanics Calculations

All molecular mechanics calculations were carried out using the AMBER* forcefield as implemented in Macromodel[20] (Version 5.0) together with the GB/SA solvation model[21] for $CHCl_3$. All calculations were performed on Silicon Graphics Indigo^2 or Power Indigo^2 computers. Conformational searching was carried out using 10000 step Monte Carlo simulations and all conformations generated within 50 kJ of the global minimum were minimised. The sets of conformations generated by these searches were then filtered appropriately using the analysis tools available within Macromodel. The data generated were exported to Deltagraph (Version 4.0.5., SPSS Inc., **1998**) for visualisation purposes.

Synthetic Procedures

Potassium 4-(Benzylcarbamato)methylbenzoate 6

Benzyl chloroformate (18.8 ml, 0.13 mol) was added in one portion to 4-(aminomethyl)benzoic acid (20 g, 0.13 mol) dissolved in 1M aqueous K_2CO_3 solution (350 ml). The mixture was left to stir overnight at room temperature and the colourless precipitate was filtered and dried under reduced pressure. The solid was slurried in refluxing acetone and water was added until the compound had dissolved. After hot filtration and cooling, **6** crystallised from solution as colourless plates (37.1 g, 87 %). m.p. >350°C (decomp); ^{1}H NMR (300 MHz,

d_6-DMSO) δ 7.85 (1H, t, $^3J_{HH}$ = 8 Hz), 7.82-7.76 (2H, m), 7.48-7.30 (5H, m), 7.19-7.10 (2H, m), 5.08 (2H, s), 4.21 (2H, d, $^3J_{HH}$ = 8 Hz); ^{13}C NMR (75 MHz, d_6-DMSO) δ 168.6, 165.9, 156.4, 140.5, 139.4, 137.2, 128.1, 127.8, 125.8, 125.6, 65.3, 43.8; MS (EI) m/z (%) 323 (M^+, 24), 191 (100); Anal. calc. for $C_{16}H_{14}NO_4K$: C, 59.43, H, 4.36, N, 4.33; Found: C, 59.55, H, 4.32, N, 4.18.

4-(Benzylcarbamato)methylbenzoyl chloride 7

Thionyl chloride (10 ml) was added dropwise to solid potassium 4-(benzylcarbamato)methylbenzoate **6** (9.38 g, 31.8 mmol) at room temperature under a positive pressure of dry N_2 gas. The reaction mixture was stirred for 24 hours until no further gas was evolved by the reaction. The thionyl chloride was removed using a water aspirator and the residue was dissolved in CH_2Cl_2, filtered, and then concentrated to dryness before being run through a pad of SiO_2 using EtOAc:CH_2Cl_2 (1:1) as eluant. The filtrate was collected and the solvent was removed from the fractions to afford **7** as a colourless solid (8.00 g, 83 %) which was used without further purification. ^{1}H NMR (300 MHz, $CDCl_3$) δ 8.01-7.98 (2H, m), 7.39-7.15 (7H, m), 5.06 (2H, s), 4.41-4.32 (2H, m); MS (EI) m/z (%) 303 (M^+, 85), 305 ($[M+2]^+$, 29), 91 (100).

2-(4'-(Benzylcarbamato)methylbenzamido)-6-methylpyridine) 8

2-Amino-6-methylpyridine (8.39 g, 85.5 mmol) was dissolved in dry CH_2Cl_2 (100 ml) and added dropwise at room temperature to solid 4-(benzylcarbamato)methylbenzoyl chloride **5** (7.82 g, 28.5 mmol) under a positive pressure of dry N_2 gas. The mixture was stirred at room temperature for a further 3 hours after which time the colourless precipitate which formed was filtered off and discarded. Hexane was added carefully to the filtrate to induce crystallisation of **8** as colourless crystals. The mother liquor was evaporated under reduced pressure and the crystallisation procedure repeated on the residue to afford further portions of **8**. (5.4 g, 79 %); m.p. 110-111°C; ^{1}H NMR (300 MHz, $CDCl_3$) δ 8.56 (1H, s), 8.23-8.16 (1H, m), 7.94-7.88 (2H, m), 7.70-7.60 (1H, m), 7.38-7.17 (7H, m), 6.96-6.89 (1H, m), 5.28-5.13 (3H, m), 4.49-4.41 (2H, m), 2.48 (3H, s); MS (EI) m/z (%) 375 (M^+, 100); HRMS found 375.1577 (M^+); Calc. for $C_{22}H_{21}N_3O_3$ 375.1583.

2-(4'-Aminomethylbenzamido)-6-pyridine 9

HBr (45% solution in AcOH, 30 ml) was added to 2-(4'-(benzylcarbamato)methylbenzamido)-6-methylpyridine) **8** (8.5 g, 24.6 mmol) in a flask fitted with a $CaCl_2$ guard tube and the reaction mixture was stirred overnight. After this time, Et_2O (400 ml) was added and the insoluble material which precipitated was collected by suction filtration and dissolved in water. The pH of this aqueous solution was adjusted to pH 9 with 2M aqueous NaOH solution. The desired product **9** crystallised from this solution as a colourless solid (5.28 g, 89 %); m.p. 159-161°C; ^{1}H NMR (300 MHz, $CDCl_3$) δ 8.52 (1H, bs), 8.21-8.18 (1H, m), 7.92-7.84 (2H, m), 7.58-7.17 (1H, m), 7.48-7.40 (2H, m), 6.98-6.88 (1H, m), 3.91 (2H, s), 2.49 (3H, s), 1.53 (2H, bs); ^{13}C NMR (75 MHz, $CDCl_3$) δ 165.4, 156.9, 150.9, 147.6, 138.8, 132.8, 127.5, 127.4, 119.4, 111.0, 46.1, 24.0; MS (EI) m/z (%) 241 (M^+, 100); HRMS found 242.1295 ($[M+H]^+$); Calc. for $C_{14}H_{16}N_3O$ 242.1293.

2-(*N*-Maleimidomethyl-4'-benzamido)-6-pyridine 1

2-(4'-Aminomethylbenzamido)-6-pyridine **9** (4.88 g, 20.2 mmol) and maleic anhydride (1.98 g, 20.2 mmol) were dissolved in dry AcOH (99+%, 30 ml) and heated to reflux for 3 hours. The acetic acid was removed under reduced pressure and the residue dried *in vacuo*. The solid residue was subjected to column chromatography (SiO_2: EtOAc:CH_2Cl_2 (1:4)) with the product eluting as the second fraction (R_f 0.45). The fractions containing

the product were combined and the solvent removed *in vacuo* to afford **1** as a colourless solid (3.43 g, 53 %). m.p. 140-141°C; ^{1}H NMR (300 MHz, $CDCl_3$) δ 8.73 (1H, bs), 8.19-8.11 (1H, m), 7.90-7.81 (2H, m), 7.65-7.56 (1H, m), 7.42-7.35 (2H, m), 6.91-6.85 (1H, m), 6.74 (2H, s), 4.70 (2H, s), 2.39 (3H, s); ^{13}C NMR (75 MHz, $CDCl_3$) δ 170.2, 165.2, 156.9, 150.8, 140.2, 138.8, 134.3, 133.9, 128.6, 127.7, 119.5, 111.1, 41.0, 23.9; MS (EI) m/z (%) 322 ([M+H]$^+$, 43), 214 (100); HRMS found 322.1198 ([M+H]$^+$); Calc. for $C_{18}H_{16}N_3O_3$ 322.1191.

2-Furylpropionic acid 2

2-Furylacrylic acid (5 g, 36 mmol) was added to a slurry of 5 % Pd on C (0.5 g) in MeOH (50 ml) under a N_2 atmosphere. The nitrogen atmosphere was exchanged for hydrogen and the mixture stirred vigorously for 5 hours. The reaction was monitored by tlc (SiO_2: CH_2Cl_2:EtOAc (1:1)) using a ceric sulfate dip to develop the plates. The reaction mixture was filtered through a Celite bed to remove the catalyst and the MeOH was removed under reduced pressure. The residue was recrystallised from water and the crystalline product further purified by sublimation under reduced pressure (50°C / 1 mmHg) to afford **2** as a colourless solid (4.4 g, 88 %). This compound should be stored in the dark at –18°C to prevent decomposition. m.p. 51-52°C (lit.[22] 58-59°C, hexane); ^{1}H NMR (300 MHz, $CDCl_3$) δ 7.35-7.25 (1H, m), 6.32-6.18 (1H, m), 6.11-5.95 (1H, m), 2.97 (2H, t, $^3J_{HH}$ = 8 Hz), 2.71 (2H, t, $^3J_{HH}$ = 8 Hz); ^{13}C NMR (75 MHz, $CDCl_3$) δ 178.5, 141.4, 129.7, 110.2, 105.6, 32.2, 23.3; MS (EI) m/z (%) 140 (M$^+$, 64), 81 (100); HRMS found 140.0478 (M$^+$); Calc. for $C_7H_8O_3$ 140.0473.

3-Furylpropionic acid 3

3-Furylpropionic acid was prepared using a procedure identical to that used for **2** and was isolated as a colourless solid. This compound should be stored in the dark at –18°C to prevent decomposition. m.p. 53-55°C (lit.[22] 64-65°C, hexane), δ_H (300 MHz, $CDCl_3$) 11.17 (1H, bs), 7.39-7.32 (1H. m), 7.28-7.22 (1H, m), 6.32-6.24 (1H, m), 2.77 (2H, t, $^3J_{HH}$ = 7 Hz), 2.62 (2H, t, $^3J_{HH}$ = 7 Hz); ^{13}C NMR (75 MHz, $CDCl_3$) δ 179.4, 143.0, 139.1, 123.2, 110.7, 34.6, 20.0; MS (EI) m/z (%) 140 (M$^+$, 54), 81 (100); HRMS found 140.0466 (M$^+$); Calc. for $C_7H_8O_3$ 140.0473.

Cycloadduct *exo*-4

1 (454 mg, 1.41 mmol) and **2** (196 mg, 1.41 mmol) were refluxed in toluene for 2 hours after which time a colourless precipitate had formed. The precipitate was collected by suction filtration and the solid then dried under reduced pressure affording the cycloadduct ***exo*-4** as a colourless solid (510 mg, 79 %); m.p. 164-165°C; ^{1}H NMR (300 MHz, d_6-DMSO) δ 12.16 (1H, bs), 10.68 (1H, s), 8.04-7.96 (3H, m), 7.77-7.69 (1H, m), 7.36-7.30 (2H, m), 7.06-7.02 (1H, m), 6.61 (1H, dd, $^3J_{HH}$ = 7 and 1.5 Hz), 6.52 (1H, d, $^3J_{HH}$ = 7 Hz), 5.15 (1H, d, $^3J_{HH}$= 1.5 Hz), 4.66 (2H, s), 3.18 (1H, d, $^3J_{HH}$= 7 Hz), 2.99 (1H, d, $^3J_{HH}$ = 7 Hz), 2.49 (3H, s), 2.63-2.02 (4H, m); ^{13}C NMR (75 MHz, d_6-DMSO) δ 176.1, 174.8, 173.8, 165.4, 156.5, 151.4, 139.7, 138.2, 137.2, 133.0, 128.2, 118.9, 111.5, 90.4, 80.0, 51.0, 50.3, 40.9, 29.6, 24.6, 23.5 (coincident peak). MS (FAB) m/z (%) 462 (M$^+$, 100), 924 ((2M)$^+$, 5); HRMS found 462.1671 (M$^+$); Calc. for $C_{25}H_{24}N_3O_6$ 462.1665.

Cycloadduct *exo*-5

1 (240 mg, 0.75 mmol) and **3** (110 mg, 0.79 mmol) were refluxed in toluene for 2 hours after which time a colourless precipitate had formed. The precipitate was collected by suction filtration and the solid then dried under reduced pressure affording the cycloadduct ***exo*-5** as a colourless solid (260 mg, 74 %); m.p. 218-210°C; ^{1}H NMR (300 MHz, d_6-DMSO) δ 12.25 (1H, s), 10.67 (1H, s), 8.01-7.97 (3H, m), 7.74-7.68 (1H, m), 7.32-7.29

(2H, m), 7.02-7.00 (1H, m), 6.12 (1H, s), 5.12 (1H, s), 5.06 (1H, s), 4.63 (2H, s), 3.11-3.02 (2H, m), 2.60-2.41 (7H, m); ^{13}C NMR (75 MHz, d_6-DMSO) δ 176.5, 176.4, 173.7, 165.6, 156.6, 151.6, 150.3, 139.9, 138.4, 133.2, 128.8, 128.3, 126.8, 119.0, 111.7, 82.5, 81.3, 49.0, 46.9, 41.2, 31.5, 23.7, 22.1; MS (FAB) m/z (%) 462 ([M+H]$^+$, 100); HRMS found 462.1667 ([M+H]$^+$); Calc. for $C_{25}H_{24}N_3O_6$ 462.1665.

Benzyl maleimide 10

Benzylamine (2.5 g, 23.4 mmol) and maleic anhydride (2.75 g, 28 mmol) were dissolved in AcOH (99+%, 40 ml) and refluxed for 2 hours. The AcOH was removed under reduced pressure and the residual solid dried *in vacuo*. The crude solid was purified by sublimation under reduced pressure (50°C / 1 mmHg) to afford **10** as a colourless solid (3.4 g, 78 %); m.p. 95-96°C (lit.[23] 94-95 °C); ^{1}H NMR (300 MHz, d_6-DMSO) δ 7.41-7.22 (5H, m), 7.08 (2H, s), 4.61 (2H, s); ^{13}C NMR (75 MHz, d_6-DMSO) δ 170.5, 136.2, 134.2, 128.7, 128.4, 127.9, 41.4. MS (EI) m/z (%) 187 (M$^+$, 100).

Cycloadduct *Exo*-11

Benzyl maleimide (140 mg, 0.75 mmol) and **2** (110 mg, 0.79 mmol) were refluxed in toluene for 2 hours after which time a colourless precipitate had formed. The precipitate was collected by suction filtration and the solid then dried under reduced pressure affording the cycloadduct ***exo*-11** as a colourless solid (211 mg, 86 %); m.p. 236-239°C; ^{1}H NMR (300 MHz, d_6-DMSO) δ 12.14 (1H, s), 7.41-7.22 (5H, m), 6.81 (1H, dd, $^3J_{HH}$ = 7.2 and 1.2 Hz), 6.57 (1H, d, $^3J_{HH}$ = 7.2 Hz), 5.19 (1H, d, $^3J_{HH}$ = 1.2 Hz), 4.66 (2H, s), 3.21 (1H, d, $^3J_{HH}$ = 6.7 Hz), 3.04 (1H, d, $^3J_{HH}$ = 6.7 Hz), 2.63-2.53 (2H, m), 2.21-2.12 (2H, m); ^{13}C NMR (75 MHz, d_6-DMSO) δ 176.2, 173.0, 164.0, 153.6, 138.9, 136.4, 134.2, 109.7, 82.5, 81.3, 49.4, 47.9, 40.2, 33.5, 22.7, 22.3; MS (EI) m/z (%) 327 (M$^+$, 100); HRMS found 327.1113 (M$^+$); Calc. for $C_{18}H_{17}NO_5$ 327.1107.

Cycloadduct *Exo*-12

Benzyl maleimide (140 mg, 0.75 mmol) and **2** (110 mg, 0.79 mmol) were refluxed in toluene for 2 hours after which time a colourless precipitate had formed. The precipitate was collected by suction filtration and the solid then dried under reduced pressure affording the cycloadduct ***exo*-12** as a colourless solid (198 mg, 81 %); m.p. 251-255°C; ^{1}H NMR (300 MHz, d_6-DMSO) δ 12.14 (1H, s), 7.43-7.27 (5H, m), 6.87 (1H, s), 5.19 (1H, s), 5.06 (1H, s), 4.66 (2H, s), 3.14 (1H, d, $^3J_{HH}$ = 6.9 Hz), 2.97 (1H, d, $^3J_{HH}$ = 6.9 Hz), 2.63-2.53 (2H, m), 2.21-2.12 (2H, m); ^{13}C NMR (75 MHz, d_6-DMSO) δ 177.2, 172.0, 166.0, 154.6, 136.9, 135.4, 134.2, 109.7, 82.1, 80.1, 49.4, 46.9, 39.2, 34.5, 24.7, 22.3; MS (EI) m/z (%) 327 (M$^+$, 100); HRMS found 327.1104 (M$^+$); Calc. for $C_{18}H_{17}NO_5$ 327.1107.

Acknowledgements

This research was supported by the University of Birmingham, the Engineering and Physical Sciences Research Council (Quota Award to A.R.), and the Biotechnology and Biological Sciences Research Council (Grants 6/B03840 and 6/B04100). We thank Prof G. von Kiedrowski for supplying us with a copy of his SimFit program.

References and Notes

[1] For general reviews, see Kirby, A.J. *Angew. Chem. Int. Ed. Engl.* **1996**, *35*, 707. Dugas, H. *Bioorganic Chemistry – A Chemical Approach to Enzyme Action*, Third Edition, Springer-Verlag, New York, **1996**. For some efficient examples, see Hosseini, M.W.; Lehn, J.M.; Jones, K.C.; Plute, K.E.; Mertes, K.B.; Mertes, M.P. *J. Am. Chem. Soc.* **1989**, *111*, 6330; Huc, I.; Pieters, J.; Rebek Jr, J. J. Am. Chem. Soc. 1994, 116, 10296; Tecilla, P.; Jubian, V.; Hamilton, A.D. *Tetrahedron* **1995**, *51*, 435.

[2] Page, M.I.; Jencks, W.P. *Proc. Nat. Acad. Sci. USA* **1971**, *68*, 1678. Page, M.I. *Chem. Soc. Rev.* **1973**, 2, 295. Kirby, A.J. *Adv. Phys. Org. Chem.* **1980**, *17*, 183. Page, M.I. in *The Chemistry of Enzyme Action*, Page, M.I. (Ed.), Elsevier, Amsterdam, **1984**, p. 1. Menger, F.M. *Acc. Chem. Res.* **1985**, *18*,128. Page, M.I. *Phil. Trans. R. Soc. Lond. B* **1991**, *332*, 149. Kirby, A.J. *Phil. Trans. R. Soc. Lond. A* **1993**, *345*, 67. Menger, F.M. *Acc. Chem. Res.* **1993**, *26*, 206.

[3] For general examples, see Kirby, A.J. *Angew. Chem. Int. Ed. Engl.* **1996**, *35*, 707. For other examples of accelerated cycloaddition reactions Kang, J.; Hilmersson, G.; Santamaria, J.; Rebek Jr., J. *J. Am. Chem. Soc.* **1998**, *120*, 7389. Kang, J.; Hilmersson, G.; Santamaria, J.; Rebek Jr., J. *J. Am. Chem. Soc.* **1998**, *120*, 3650. Marty, M.; Clyde-Watson, Z.; Twyman, L.J.; Nakash, M.; Sanders, J.K.M. *Chem. Commun.* **1998**, 2265. Hamilton, A.D.; Hirst, S.C. *J. Am. Chem. Soc.* **1991**, *113*, 382. Kelly, T.R.; Ekkundi, V.S.; Meghani, P. *Tetrahedron Lett.* **1990**, *31*, 3381. Mock, W.L.; Irra, T.A.; Wepsiec, J.P.; Adhya, M. *J. Org. Chem.* **1989**, *54*, 5302. Mock, W.L.; Irra, T.A.; Wepsiec, J.P.; Manimaran, T.L. *J. Org. Chem.* **1983**, *48*, 3619.

[4] In order to distinguish between transition state effects and ground state effects, we will use the description *accelerated* when the rate of a reaction is enhanced by the lowering of the energy of the transition state by a recognition event and the description *facilitated* when the extent of reaction is enhanced by the lowering of the energy of the product by a recognition event.

[5] For preliminary communications on recognition-mediated acceleration and control of cycloaddition reactions, see Philp, D.; Robertson, A. *Chem. Commun.* **1998**, 879. Booth, C.A.; Philp, D. *Tetrahedron Lett.* **1998**, *39*, 6987.

[6] For a review of the use of furan Diels-Alder chemistry in synthesis, see Kappe, C.O.; Murphree, S.S.; Padwa, A. *Tetrahedron* **1997**, *53*, 14179. For reviews of intramolecular Diels-Alder reactions, see Brieger, G.; Bennett, J.N. *Chem. Rev.* **1980**, *80*, 63. Fallis, A.G. *Can. J. Chem.* **1984**, *62*, 183. Ciganek, E. *Org. React.* **1984**, *32*, 1. Craig, D. *Chem. Soc. Rev.* **1987**, *16*, 187. Fallis, A.G. *Acc. Chem. Res.* In press. For some recent examples of intramolecular Diels-Alder reactions, see Carreno, M.C; Ruano, J.L.G.; Urbano, A. *J. Org. Chem.* **1996**, *61*, 6136. Millan, D.S.; Pham, T.T.; Lavers, J.A.; Fallis, A.G. *Tetrahedron Lett.* **1997**, *38*, 795. Lilly, M.J.; Sherburn, M.S. *Chem. Commun.* **1997**, 967. Wong, T.; Wilson, P.D.; Woo, S.; Fallis, A.G. *Tetrahedron Lett.* **1997**, *38*, 7045. Bush, E.J.; Jones, D.W. *J. Chem. Soc., Perkin Trans. 1* **1997**, 3531.

[7] Stereoselective Diels-Alder reactions can be performed in the presence of chiral Lewis Acids. For some recent examples, see Bruin, M.E.; Kundig, E.P. *Chem. Commun.* **1998**, 2635. Bromidge, S.; Wilson, P.C.; Whiting, A. *Tetrahedron Lett.* **1998**, *39*, 8905. Ishihara, K.; Kurihara, H.; Matsumoto, M.; Yamamoto, H. *J. Am. Chem. Soc.* **1998**, *120*, 6920. Hubbard, R.D.; Miller, B.L. *J. Org. Chem.* **1998**, *63*, 4143. Bienamye, H. *Angew. Chem. Int. Ed. Engl.* **1997**, *36*, 2670.

[8] For a catalytic method of accelerating the rate of an intramolecular Diels-Alder reaction based on hydrogen bonding, see Hirst, S.C.; Hamilton, A.D. *J. Am. Chem. Soc.* **1991**, *113*, 382. For a catalytic method of accelerating the rate of an intermolecular Diels-Alder reaction, see Walter, C.J.; Sanders, J.K.M. *Angew. Chem. Int. Ed. Engl.* **1995**, *34*, 217. In the present context, we are not concerned with catalysis, but rather ensuring that, by encoding the appropriate recognition features within the reagents, the Diels-Alder reaction is accelerated and its stereochemical outcome controlled.

[9] Boissonnas, R.A.; Guttmann, S.; Huguenin, R.L.; Jaquenold, P.A.; Sandrin, E. *Helv. Chim. Acta* **1958**, *41*, 1867.

[10] The assignment of *endo* or *exo* stereochemistry to the cycloadducts was made on the basis of 500 MHz ^{1}H NMR experiments conducted in $CDCl_3$ solution at room temperature on a sample of **5** which contained only one of the two stereoisomers. In order to assign the stereochemistry of the cycloadduct, our attention focussed on the through bond coupling and nOe relationships displayed by the doublet ($^3J_{HH}$ = 1.5 Hz) centred on δ 5.18. This resonance can be assigned to that arising from the bridgehead proton of the cycloadduct. It is accepted that in the oxabicyclo[2.2.1]heptene skeleton, generated by cycloadditions involving furans, that the bridgehead proton will display a large $^3J_{HH}$ to a proton in the *exo* position whereas it will display a very small $^3J_{HH}$ to a proton in the *endo* position. In other words, one might expect the *exo* cycloadduct to display little or no coupling between the bridgehead proton and the *endo* protons in the oxabicyclo[2.2.1]heptene skeleton, and, conversely, one might expect the *endo* cycloadduct to display a large three bond between the bridgehead proton and the *exo* protons in the oxabicyclo[2.2.1]heptene skeleton. In the case of **5**, the 1.5 Hz coupling observed in the resonance at δ 5.18 could be assigned by COSY experiements to coupling between the bridgehead proton and one of the alkene protons of the oxabicyclo[2.2.1]heptene skeleton. This observation implies that the sample contains a cycloadduct with *exo* stereochemistry. This tentative assignment was confirmed by gradient nOe experiments which demonstrated a pattern of nOes which were consistent only with exo stereochemistry. The assignments of stereochemistry to the cycloadducts **4**, **11** and **12** were performed by analogy with the assignment for **5** described above.

[11] The equilibrium or thermodynamic effective molarity is defined as the equilibrium constant for the intracomplex reaction (K_{RM}) divided by the equilibrium constant (K_{bi}) for the bimolecular reaction. Thus, for the *exo* isomers, the thermodynamic EM is given by k_2k_5/k_1k_6 and for the *endo* isomers, the kinetic EM is given by k_4k_7/k_3k_8.

[12] The kinetic effective molarity is defined as the rate constant for the intracomplex reaction divided by the rate constant for the bimolecular reaction. Thus, for the *exo* isomers, the kinetic EM is given by k_5/k_1 and for the *endo* isomers, the kinetic EM is given by k_7/k_3.

[13] When the course of the reaction between **1** and **2** was monitored in $CDCl_3$ at 30°C from initial concentrations of the reactants of 40 mM, the observed rate of reaction was approximately equal to that of the control reaction between **2** and **10**. This observation is entirely consistent with the calculated value for the kinetic EM of around 40 mM.

[14] Molecular mechanics calculations suggest that the source of this reversal of stereoselectivity is an intramolecular hydrogen bon between the carboxylic acid and one of the carbonyl oxygen atom of the imide in the *endo* cycloadduct.

[15] An amide NH proton typically exhibits a downfield chemical shift change of between 2 and 3 ppm when participating in a hydrogen bond with a carbonyl oxygen atom. In this case, it is important to note that

***exo*-5** can participate in *inter*molecular hydrogen bonding, and so we would expect a downfield shift of its amide NH resonance to be observed. This chemical shift change will tend to reduce the observed difference in chemical shifts between the amide NH resonances of ***exo*-5** and ***endo*-5**, which can form an *intra*molecular hydrogen bond. Hence, the observed chemical shift difference between the amide NH resonances of ***endo*-5** and ***exo*-5** of >1.4 ppm is highly significant

[16] Armarego, W.L.F.; Perrin, D.D. *Purification of Laboratory Chemicals*, Fourth Edition, Butterworth Heinemann, Oxford, **1997**.

[17] *SimFit*, A Program for the Analysis of Kinetic Data, Version 1.0, von Kiedrowski, G., **1994**.

[18] Wilcox, C.S., in *Frontiers in Supramolecular Organic Chemistry and Photochemistry*, Schneider, H.J.; Dürr, H. (Eds), VCH, Weinheim, **1991**, p. 123.

[19] Fitting of the 1:1 binding isotherm to the experimental data was accomplished using a set of custom-designed spreadsheets developed for Excel 97/98. Copies of these spreadsheets, which require the Solver add-in for Excel, are available on request from the author.

[20] Mohamadi, F.; Richards, N.G.J.; Guida, W.C.; Liskamp, R.; Lipton, M.; Caufield, C.; Chang, G. Hendrickson, T.; Still, W.C. *J. Comput. Chem.* **1990**, *11*, 440.

[21] Still, W.C.; Tempczyk, A.; Hawley, R.C.; Hendrickson, T. *J. Am. Chem. Soc.* **1990**, *112*, 6127.

[22] Arena, G.; Cali, R.; Maccarone, E.; Passerini, A. *J. Chem. Soc., Perkin Trans. 2* **1993**, 1941.

[23] Hearn, D.; Ward, K. *Aust. J. Chem.* **1977**, *30*, 203.